ARTICLES

Electronic States at the Water/Air Interface†

Javier Rodriguez‡ and Daniel Laria*,‡,§

Unidad Actividad Química, Comisión Nacional de Energía Atómica, Avenida Libertador 8250, 1429 Buenos Aires, Argentina, and Departamento de Química Inorgánica, Analítica y Química-Física e INQUIMAE, Facultad de Ciencias Exactas y Naturales, Universidad de Buenos Aires, Ciudad Universitaria, Pabellón II, 1428 Buenos Aires, Argentina

Received: March 2, 2004; In Final Form: May 6, 2004

Using combined path integral−molecular dynamics simulation techniques, we analyze electronic solvation at the water/air interface. Superficial electrons present a considerable extent of spatial confinement, somewhat less marked but still comparable to that found in bulk. The characteristics of the interfacial polarization promote an overall structure for the solvated electron−polymer which looks flatter along the direction perpendicular to the interface. Spatial and orientational responses of different slabs in the close vicinity of the interface were also investigated. Solvent configurations obtained from the simulations have been used to analyze electronic excited states and the optical absorption spectrum of superficial electrons. Compared to bulk results, the distribution of bound electronic states at the surface presents similar characteristics, that is, a ground s-state and three, quasi-degenerate, p-like excited states. The reduction of the energy gap between the ground state and the rest of excited states leads to a ∼0.52 eV red-shift in the position of the absorption maximum.

I. Introduction

In this article, we will focus on excess electrons adsorbed at the water/air interface. In a broader context, the subject is akin to that of surface ionic solvation,[1−4] which is of fundamental importance in a wide variety of problems related to chemical reactivity in aerosols, atmospheric chemistry, electrochemistry, and heterogeneous catalysis as well.[5−9] Perhaps the most clear feature that distinguishes bulk from interfacial environments is the lack of translational symmetry in the latter. From the microscopic point of view, the reduction in dimensionality gives rise to large anisotropies in the force fields that drive the dynamics of the particles; these modifications, in turn, lead to changes in interparticle connectivity patterns,[10,11] orientational correlations,[12] and alterations in the single molecule and collective dynamical modes as well.[13−17]

The subject of ionic solvation at interfaces still continues to draw considerable attention. Despite their apparent simplicity, key issues such as those pertaining to local concentration fluctuations for interfacial ionic species have remained elusive until very recently. At present, there seems to be sufficient evidence that subtle details related to polarization fluctuations in both the interface and the solute species may lead indistinctly to depletions or enhancements in the local ionic concentrations at interfaces.[4]

Solvated electrons are very sensible ionic probes in solution chemistry. The analysis of steady-state and time-resolved electronic spectroscopies gives access to detailed information about the changes that operate in the structure of liquids to accommodate negatively charged solute species. Moreover, effects arising from the intrinsic quantum nature of the electrons introduce new features in the description of the solvation process, most notably, those related to the electron delocalization/localization transition. One clear manifestation of this phenomenon is given by the dramatic changes in the electron transport properties as one varies, for example, the density of the host fluid.[18] Over the last 40 years, a large body of experimental and theoretical work has been devoted to the analysis of electron solvation in a wide variety of polar and nonpolar liquids.[19,20] For the particular case of aqueous environments, the list includes water at ambient conditions,[21−28] hot water,[29−32] supercritical states of water,[33−37] and also water nanoclusters.[38−40] Yet, a detailed analysis of electrons adsorbed at aqueous interfaces is still lacking.

It has been known for quite a long time that liquid/vapor interfaces can support electronic states; the particular case of low-temperature helium is one classical example.[41−44] From the theoretical point of view, the analysis of these electronic superficial states has normally been performed within the framework of continuum models, where the localization of the electron is operated by an image charge potential acting on the electron, along directions perpendicular to the interface. More recently, two photon photoemission experiments have also provided experimental proof of interfacial electronic solvation in a wide variety of metal/polar and metal/nonpolar slab interfaces at ambient conditions.[45−49] Basically, these experiments involve an initial electron pumping from below the corresponding Fermi level of the metal into the liquid slab. A delayed second probe pulse analyzes the evolution of the subsequent electronic dynamics and the response of the interface as the electron normally gets localized. The electronic localization is the result of a self-trapping process that resembles, in some aspects, similar

† Part of the special issue "David Chandler Festschrift".

* To whom correspondence should be addressed. E-mail: dhlaria@cnea.gov.ar.

‡ Comisión Nacional de Energía Atómica.

§ Universidad de Buenos Aires.

10.1021/jp049058g CCC: $30.25
Published on Web 10/02/2004

processes that take place after the photoinjection of electrons in bulk liquid phases.[28] Snee et al.[50] have just performed a mixed quantum-classical simulation study of the electronic solvation dynamics at the methanol/platinum interface.

With a similar spirit, in this paper, we present a computer simulation analysis of electrons adsorbed at the liquid/air interface using a combined path integral−molecular dynamics (PIMD) approach. Our main goal is to establish distinctive features between these states and those prevailing in bulk phases. To that end, we have analyzed the extent of the spatial localization of superficial electrons and the characteristics of the electron−solvent spatial correlations. Modifications in the polarization structure of the clean interface induced by the presence of the electron were also examined. Finally, we have investigated electronic excitations by computing the electronic density of states and the optical absorption spectrum.

The outline of this work is as follows: In section II, we present details of the model and the simulation methodology; results from the PIMD runs and the analysis of the electronic density of states and absorption spectrum are presented in section III. The concluding remarks are left for section IV.

II. Model

Simulation experiments were performed on a system composed by one electron lying at one of the liquid/air interfaces of an aqueous slab, composed by $N_w = 342$ water molecules. The slab was originally constructed by suppressing periodic boundary conditions along the *z*-axis in a previously equilibrated, fully periodic aqueous system of density 1 g cm^{-3}, containing one electron. The localization of one of the interfaces was initially adjusted so as to roughly coincide with z_c, the *z*-coordinate of the electron centroid. A precise definition of the centroid will be given below.

The potential energy of the system included water−water and water−electron contributions. The former was considered as a sum of pairwise intermolecular interactions that included site−site Lennard-Jones and Coulomb interaction terms. To describe the geometry and charge distribution of the water molecules, the simple point charge (SPC) model by Berendsen et al.[52] was adopted. Electron−water interactions were modeled using the pseudopotential developed by Turi et al.,[25,51] that incorporates the correct electrostatics, local repulsion, local exchange, and polarization contributions as well. This pseudopotential has been tested in a wide variety of aqueous environments and reproduces the energetics and the absorption spectra of solvated electrons reasonably well.[30] In all cases, Lennard-Jones interactions were neglected for distances beyond 10.5 Å. Long-ranged interactions derived from the different Coulomb terms were handled by implementing Ewald sum techniques for slab geometries,[53] assuming the presence of a uniform neutralizing background.

Our statistical mechanical approach to analyze the behavior of the electron at the interface was based on Feynman's path integral formalism.[54] The simulation methodology relies on the well-known isomorphism[55] that can be established between the statistics of the electron quantum path and that of a classical ring polymer containing *P* "beads" with coordinates $\mathbf{r}_i$, interacting with nearest neighbor harmonic couplings. With the exception of the electron, quantum fluctuations were neglected in the rest of the solvent particles. Equilibrium configurations for the superficial solvation of the electron−polymer were generated using combined PIMD techniques. The trajectories corresponded to canonical runs at a temperature $T = 298$ K. In this thermal regime, the slab presented a stable structure, with negligible evaporation during the course of the simulations. The number of electron beads was set to $P = 1000$. Additional details of the simulation procedure can be found in refs 37 and 56.

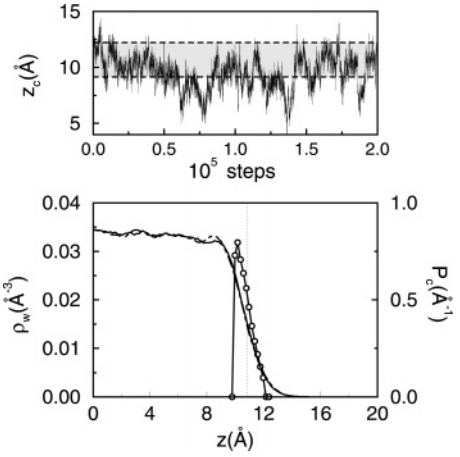

Figure 1. Bottom panel: Density profile (solid line, left axis) for the water slab and probability density P_c (open circles, right axis). The dotted line represents the position of the Gibbs dividing surface. To facilitate the comparison between the two interfaces, the negative *z*-portion of the water density appears in the positive axis (dashed line). Top panel: Unconstrained trajectory for z_c. The shaded area corresponds to the width *l* of the interface (see the text).

III. Results

A. Electron Solvation. To gain a qualitative insight into the characteristics of the electron solvation at the water/air interface, it will be useful to first examine the gross features of the structure of the simulated slab. In the bottom panel of Figure 1, we present results for the average water density $\rho_w(z)$ defined by

$$\rho_w(z) = \frac{1}{A}\left\langle \sum_{i=1}^{N_w} \delta(Z_i - Z_{CM} - z) \right\rangle \qquad (1)$$

where $\langle ....\rangle$ denotes an equilibrium average and Z_{CM} and Z_i represent the *z*-coordinates of the centers of mass the slab and the *i*th water molecule, respectively. $\rho_w(z)\,dz$ represents the number of water molecules per unit of area *A* in the *x*−*y* plane, with their centers of mass lying between *z* and $z + dz$. The average local density at the central part of the slab $\bar{\rho}_w$ was close to the usual bulk value of water at ambient conditions, $\rho_w(z = 0) = 0.034$ Å^{-3}. The two Gibbs dividing surfaces were located at ±10.8 Å measured from Z_{CM}. At a first glance, the two interfaces present similar shapes, with characteristic widths of the order of $l \sim 3$ Å, defined according to the 10%−90% density criterion.

The water/air interface represents a nonuniform environment for the electron solvation. A phase-space trajectory for z_c is presented in the top panel of Figure 1. Within the discretized picture of the electron−polymer, that coordinate is defined as $z_c = 1/P\sum_i^P z_i$. In the course of a fairly long trajectory of 2×10^5 simulation steps, which is well beyond the characteristic decorrelation interval of most of the physical observables associated with the interface, one observes that the sampling includes both superficial and bulk electronic states. Note that the fluctuations in z_c are comparable to or even larger than two relevant length scales of the problem under consideration: (i) the width of the interface *l* and (ii) the typical size of an aqueous electron in bulk water which, at ambient conditions, is intermediate between 3 and 4 Å. Consequently, a fully unrestricted sampling for the electron−polymer is likely to include contribu-

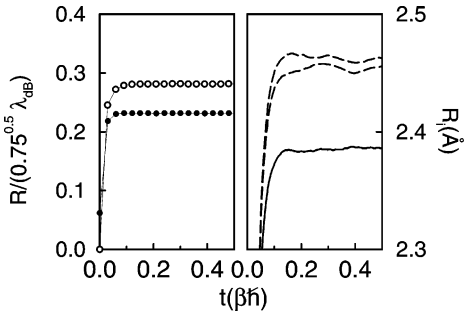

Figure 2. Left panel: Root-mean-square correlation function for aqueous electrons at $T = 298$ K: superficial states (open circles); bulk results (black circles). Right panel: Root-mean-square correlation along the *z*-direction (solid line) and the *x*- and *y*-directions (dashed lines).

tions from microenvironments exhibiting well-differentiated structural characteristics. This includes limiting states that can be ascribed to liquid, gaslike, and the manifold of intermediate superficial states as well. To single out the latter contributions, we focused attention on solvation in the close vicinity of the Gibbs dividing surface. This was achieved by supplementing the Hamiltonian of the system with an extra confining potential term, V_{cf}, acting on the electron centroid, that restricted the sampling of electronic states within a rectangular slab of width $\Delta = 2$ Å, centered at $z_s = 11$ Å. This procedure has been implemented in the past to analyze superficial states of classical solutes.[1,2,57] Following these previous studies, V_{cf} was chosen of the form[2]

$$V_{cf}(z_c) = k\xi^3 H(\xi) \qquad \xi = |z_c - Z_{CM} - z_s| - \frac{1}{2}\Delta \quad (2)$$

where H is the Heaviside function. The restoring force constant k was set to 10^4 kcal/mol Å^{-3}.

The bottom panel of Figure 1 also includes results for the probability density associated with the position of the electron centroid:

$$P_c(z) = \langle \delta(z_c - Z_{CM} - z) \rangle \quad (3)$$

using the above-mentioned, restricted sampling scheme. Similarly to what has been found in the case of classical anions,[2] the histogram of the centroid position is not uniform across the sampling window and reflects a propensity of the electron to reside near the inner edge of the slab. Nevertheless, the average value of z_c was reasonably close to the position of the Gibbs dividing surface, $\langle z_c \rangle = 10.6$ Å.

The equivalence between the electron path and the isomorphic ring polymer provides a convenient geometrical interpretation of the extent of spatial localization of the electronic states. The key magnitude to analyze in this context is the correlation length of the electron−polymer $\mathscr{R} = \mathscr{R}(\beta\hbar/2)$, where $\mathscr{R}^2(t)$ represents the second moment of the intramolecular distribution of the electron−polymer, namely,

$$\mathscr{R}^2(t - t') = \langle |\mathbf{r}(t) - \mathbf{r}(t')|^2 \rangle \qquad 0 \le t - t' \le \beta\hbar \quad (4)$$

In the previous equation, $\mathbf{r}(t)$ represents the electron position at imaginary time t and the rest of the symbols retain their usual meanings. In the left panel of Figure 2, we present results for $\mathscr{R}(t)$ for superficial and bulk electronic solvation. Note that from a qualitative point of view, the presence of a plateaulike behavior in the time dependence of $\mathscr{R}(t)$ for $t > 0.1\beta\hbar$ reveals ground state dominance in the interfacial solvation of the electron.[58] The extent of spatial localization expressed in terms of $\mathscr{R}$ is somewhat less marked at the surface than in bulk. Anyhow, the resulting sizes in both cases are well below the electronic de Broglie thermal wavelength, which roughly corresponds to the free (i.e., noninteracting) result, $\mathscr{R}_f = (0.75)^{1/2}\lambda_{dB} \sim 15$ Å. Incidentally, also note that the size of the superficial electron−polymer $\mathscr{R}/\mathscr{R}_f \sim 0.28$ is comparable to that found for superficial electrons adsorbed at nanoclusters of the type $[H_2O]_n$, with n as small as 32, $\mathscr{R}/\mathscr{R}_f \sim 0.26$.[40] Although both estimates may be still dependent on Hamiltonian details, they would indicate that polarization fluctuations in small nanoclusters retain similar "effectiveness" in promoting superficial electronic localization to that observed at the interfaces of bulk phases.

The anisotropy induced by the presence of the interface also leads to differences in the spatial localizations along directions perpendicular and parallel to the interface. In the right panel of Figure 2, we present results for $\mathscr{R}_i(t)$ defined as

$$\mathscr{R}_i^2(t - t') = \langle |x_i(t) - x_i(t')|^2 \rangle \quad (5)$$

for $i = x, y, z$. For bulk water, $\mathscr{R}_i = \mathscr{R}/\sqrt{3} \sim 1.9$ Å for all i; instead, at the interface, $\mathscr{R}_z = 2.38$ Å, a value which is somewhat smaller than $\mathscr{R}_i \sim 2.45$ Å for $i = x, y$. Also note that the spatial anisotropy in the overall polymer shape could also have been anticipated from the analysis of the potential energy surface associated with the adsorbed electron. In Figure 3, we present a contour plot for the electron−interface coupling across the $x = 0$ plane, for a typical configuration of superficial electronic solvation. The presence of steeper gradients along the *z*-axis compared to those along the perpendicular *y*-direction is accordant to the above-mentioned electron−polymer structure. The resulting solvation structure that emerges from these considerations can be pictured as an interface polarization arrangement benefitting a moderately oblate electron−polymer adsorbed at the surface. From the energetic point of view, this structure would be more favorable than an isotropic one, since it allows a larger "contact area" between the adsorbed electron and the interfacial solvent.

B. Surface Responses. Having characterized intrapolymer spatial correlations for superficial electrons, we now turn to the analysis of the spatial and orientational responses of the interface. The first function that will be considered is the centroid−solvent pair correlation functions defined as

$$\bar{\rho}_w g_{c\alpha}(r) = \frac{1}{4\pi r^2}\left\langle \sum_i \delta(|\mathbf{r}_c - \mathbf{R}_i^\alpha| - r) \right\rangle \quad (6)$$

where $\mathbf{R}_i^\alpha$ denotes the coordinate of site $\alpha = O, H$ in the ith water molecule. In Figure 4, we present results for $g_{c\alpha}$ for superficial and bulk environments. The latter coincides reasonably well with results from adiabatic dynamics−molecular dynamics experiments[51] and previous path integral studies using a different electron−water pseudopotential.[24] The ~1 Å shift between the positions of the first maxima of g_{cO} and g_{cH} and the corresponding running integrals would indicate that the first solvation shell in bulk consists of five water molecules, four of them coordinated to the electron via linear hydrogen bonds. The direct comparison between the two sets of plots shows a sensible reduction in the degree of solvent structure for the case of superficial electrons: The two main peaks look somewhat broader, and the overall position for the case of hydrogen is shifted approximately 0.5 Å toward larger distances. The running integrals over the oxygen and hydrogen distributions show a trend opposite to that described for bulk, with a deficit of approximately ~0.5 O atoms with respect to H atoms. In

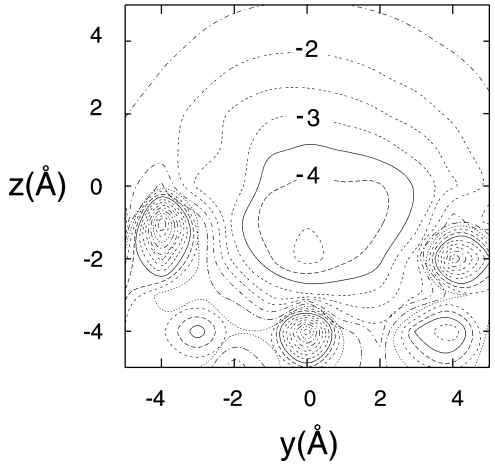

Figure 3. Contour plot for the interface−electron potential energy surface (in eV) across the $x = 0$ plane. The origin of coordinates coincides with the position of the electron centroid.

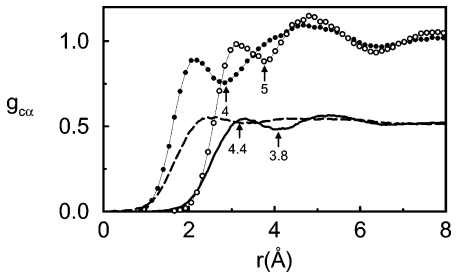

Figure 4. Electron centroid−water pair correlation functions for superficial states: g_{cO} (solid line); g_{cH} (dashed line). Also shown are results for bulk electronic solvation: g_{cO} (open circles); g_{cH} (black circles). The arrows indicate site populations under the first peaks.

principle, these results would reflect changes in the electron−water connectivity, from linear hydrogen bonds in bulk toward a "dipolar-like" pattern that would prevail at the interface. Finally, note that the differences between the local solvent site densities in bulk and surface states are much smaller than the trivial factor ∼0.5, arising for the reduction of the average local density at the interface.

There are two sources of solvent spatial inhomogeneity in the close vicinity of the electron: (i) the radial electric field generated by the excess charge and (ii) the presence of the interface, that breaks the isotropy that would prevail in bulk environments. Results from by $g_{c\alpha}$, being spherically averaged, do not capture the latter effects. To gain further insight about the interfacial responses, we found it appropriate to analyze two-dimensional correlations restricted to superficial slabs of width Δ. To describe electron−solvent density correlations within the slabs, we computed the following functions:

$$\bar{\rho}_j G_j(r) = \frac{1}{2\pi r \Delta}\left\langle \sum_i \delta(|\mathbf{r}_c - \mathbf{r}_i^O| - r) H(z_i^O; \bar{z}_j)\right\rangle \qquad (7)$$

where $H(z_i^O; \bar{z}_j)$ represents the characteristic function for the j slab centered at $\bar{z}_j$. H was defined as 1 if the z coordinate of the ith oxygen satisfies $|z_i^O - Z_{CM} - \bar{z}_j| < \Delta$ and 0 otherwise; $\bar{\rho}_j$ is the average density within the slab. Three different superficial slabs centered at $\bar{z}_1 = 9$ Å ($\bar{\rho}_1 = 0.91\bar{\rho}_w$), $\bar{z}_2 = 11$ Å ($\bar{\rho}_2 = 0.40\bar{\rho}_w$), and $\bar{z}_3 = 13$ Å ($\bar{\rho}_3 = 0.05\bar{\rho}_w$) were analyzed. As such, microscopic structures within the first slab should resemble very much those of a typical denser liquid aqueous state, while in the last slab, the scenario that prevails should be much closer to what is normally perceived as a vaporlike environment. In

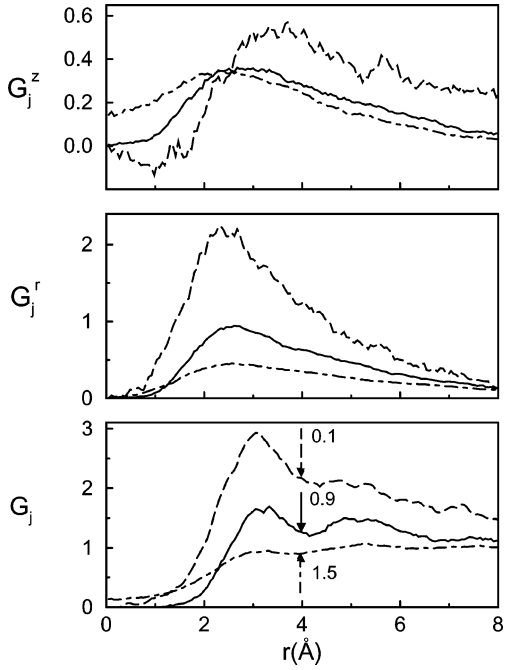

Figure 5. Spatial and orientational correlations for different superficial slabs. Electron−oxygen density correlation functions (bottom panel), local polarization densities along radial directions (middle panel), and local polarization densities along the z-axis (top panel). Results for slabs 1−3 are represented by solid, dotted−dashed, and dashed lines, respectively.

the bottom panel of Figure 5, we display results for $G_j(r)$. As expected, density fluctuations become stronger as we move from dense to more dilute slabs; however, contributions to the solvent population in the first solvation shell from the outer slab are practically negligible. The three curves show some degree of structure (much more noticeable in the intermediate slab case) at $r \sim 4$ Å, a distance that roughly coincides with the boundary of the first solvation shell of the superficial g_{cO} (cf. Figure 4).

The characteristics of the local polarization density along radial directions centered at the electron position were analyzed through the function $G_j^r(r)$, defined as

$$\bar{\rho}_j G_j^r(r) = \frac{1}{2\pi r \Delta}\left\langle \sum_i \delta(|\mathbf{R}_i^O - \mathbf{r}_c| - r)\cos(\theta_i^r) H(z_i; \bar{z}_j)\right\rangle$$

$$\cos(\theta_i^r) = \frac{\boldsymbol{\mu}_i \cdot (\mathbf{r}_c - \mathbf{R}_i^O)}{|\boldsymbol{\mu}_i||\mathbf{r}_c - \mathbf{R}_i^O|} \qquad (8)$$

where μ_i represents the dipole moment of the ith water molecule. Similarly, information about the local solvent polarization along directions perpendicular to the interface can be obtained from the following function:

$$\bar{\rho}_j G_j^z(r) = \frac{1}{2\pi r \Delta}\left\langle \sum_i \delta(|\mathbf{r}_c - \mathbf{R}_i^O| - r)\cos(\theta_i^z) H(z_i; \bar{z}_j)\right\rangle$$

$$\cos(\theta_i^z) = \frac{\boldsymbol{\mu}_i \cdot \hat{\mathbf{z}}}{|\boldsymbol{\mu}_i|} \qquad (9)$$

where $\hat{\mathbf{z}}$ represents the unit vector along the z-direction. The middle and upper panels of Figure 5 display results for these orientational correlations. All radial polarization curves present similar characteristics: Main peaks located at ≈2.3 Å, followed by monotonic decays toward zero at large distances. These tails can be reasonably well described by single exponentials with

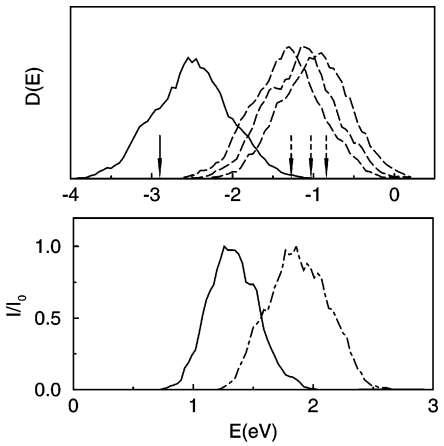

Figure 6. Top panel: Density of bound electronic states for superficial electrons. The arrows indicate the maxima of the density of states for bulk electronic states. Bottom panel: Ground-state absorption spectrum for superficial states (solid line). The absorption spectrum for bulk water is also shown (dotted−dashed line).

characteristic length scales, intermediate between 2 and 4 Å, that become larger as we move from the outer slab toward the inner one. On the other hand, the curves for the polarization along the *z*-axis are qualitatively different. First, we recall that polarization in clean water interfaces is mostly perpendicular to the *z*-axis, so $G_j^z(r)$ should be close to zero as $r \rightarrow \infty$.[59] For the outer slab, a simple geometrical construction suffices to explain that the negative portion of the curve for $r < 2$ Å is accordant to the radial alignment of dipoles of water molecules with coordinates $z_i^{\mathrm{O}} > z_c$. For the middle slab, the results would suggest that the electron−solvent coordination involves typically one water molecule with one hydrogen pointing toward the electron and the second toward the surface, leading to $\cos(\theta_i^z) > 0$.

In addition, integrals over the distributions provide quantitative estimates of the magnitude of the overall local polarizations in different slabs:

$$g_j^i = \bar{\rho}_j \int_{\Gamma_j} G_j^i(r)\, \mathrm{d}\mathbf{r} \tag{10}$$

where the integrals are restricted to the volume of the *j*th slab, Γ_j. Taking the value for the intermediate slab as a reference, we get $g_1^r/g_2^r = 0.23$ and $g_3^r/g_2^r = 1.42$; similarly, $g_1^z/g_2^z = 0.27$ and $g_3^z/g_2^z = 1.7$. In both cases, we observe similar trends, with net polarizations decreasing as we move toward outer slabs.

C. Absorption Spectrum of Superficial Electrons. Solvent configurations obtained from the PIMD experiments were also used to obtain additional information pertaining to electronic excitations at the interface. Following the procedure described in ref 30, we computed electronic eigenstates ψ_n and eigenvalues ϵ_n for 500 statistically uncorrelated solvent configurations. In brief, the electronic eigenstates were constructed as linear combinations of a basis set of three-dimensional Gaussian functions according to

$$\psi_n(\mathbf{r}) = \sum_{i=0} c_i^n\, \phi_i(\mathbf{r}) \qquad \phi_i(\mathbf{r}) = \left(\frac{2\alpha}{\pi}\right)^{3/4} \mathrm{e}^{-\alpha(\mathbf{r}-\mathbf{r}_i)^2} \tag{11}$$

The centers of the Gaussian basis $\mathbf{r}_i$ were located in a cubic grid, centered at the original position of the electron centroid. The number of basis was set to 7^3 points. The spacing of the grid was 1.45 Å, and the widths of the Gaussian basis were taken to be $\alpha = 0.36$ Å^{-2}. Within this scheme, the diagonalization procedure reduces to the solution of a generalized eigenvalue problem for the unknown set of coefficients $\{c_i^n\}$. The simple functionality of the electron−water pseudopotential adopted here, combined with the use of the Gaussian basis, facilitates the analytical evaluation of practically all contributions to the matrix elements. Additional technical details of the diagonalization procedure can be found in ref 30.

Figure 6 shows results for $D(E)$, the electron density of bound states defined as

$$D(E) = \left\langle \sum_{\epsilon_i<0} \delta(\epsilon_i - E) \right\rangle \tag{12}$$

for superficial electrons at ambient conditions. The distribution of bound states is typically composed by the ground, s-like state lying at energies intermediate between −3 and −2 eV and three, almost degenerate, p-like excited states at energies close to ca. −1 eV. Estimates for the size of these states were computed using

$$\sigma_i^2 = \langle \psi_i | (\mathbf{r} - \bar{\mathbf{r}}_i)^2 | \psi_i \rangle \tag{13}$$

with $\bar{\mathbf{r}}_i = \langle \psi_i | \mathbf{r} | \psi_i \rangle$. Our simulations yield averaged values of $\sigma_0 = 3.6$ Å and $\sigma_i = 4.3 \pm 0.1$ Å for $i = 1, 2, 3$. For the sake of comparison, we have also included in Figure 6 the position of the maximum of the distribution for bulk aqueous electrons. Note that the main effects in passing from bulk to surface solvation involve a ∼0.5 eV shift of ϵ_0 toward higher energies, while the positions for the rest of the excited states remain practically unchanged. The reduction of the gap can be easily interpreted as a direct consequence of larger spatial extents of the superficial electrons compared to the bulk situation. The ground-state absorption spectra, $I(E)$, calculated within the Franck−Condon approximation complete our analysis. It was computed using the expression

$$I(E) \propto E(1 - \mathrm{e}^{-\beta \mathrm{E}}) \left\langle \sum_{i>0,\epsilon_i<0} |\langle \psi_0 | \mu | \psi_i \rangle|^2\, \delta(\epsilon_i - \epsilon_0 - E) \right\rangle \tag{14}$$

and is presented in Figure 5, where we have also included PIMD results for bulk. The comparison between the two curves shows the following features: (i) In accordance with the observed reduction of the energy gap in the density of states, there is a ≃0.52 eV red-shift in the positions of the maxima, namely, $E_{\max}^{\mathrm{bulk}} \simeq -1.87$ eV and $E_{\max}^{\mathrm{surf}} \simeq -1.35$ eV. (ii) The normalized width at half-height of the band for surface states, $\Delta E/|E_{\max}^{\mathrm{surf}}| \sim 0.43$, is somewhat larger compared to the value obtained in bulk, $\Delta E/|E_{\max}^{\mathrm{bulk}}| \sim 0.32$, revealing relative larger fluctuations in the sizes of the electron localization traps at the interface. (iii) Both simulated line shapes present profiles that can be reasonably well described by a single Gaussian fit. In this respect, our results fail to capture the asymmetry of the experimental line shape of the spectrum of solvated electrons in bulk water.[26]

IV. Concluding Remarks

We have presented a microscopic analysis of solvated electrons in the vicinity of the Gibbs dividing surface of the water/air interface. The main results of the article can be summarized as follows: Surface polarization fluctuations at the water/air interface are sufficiently strong so as to promote a considerable extent of spatial localization of the excess electrons; the resulting size of the isomorphic electron−polymer is about 20% larger than that characterizing excess electrons in bulk

water. Moreover, the anisotropy in the force fields at the interface leads to an overall polymer structure that is slightly flatter along directions perpendicular to the interface.

Analysis of the electron−water density fields in the close vicinity of the superficial electron reveals that the first solvation shell is composed roughly by four water molecules. Three of these molecules lie within 2 Å of the Gibbs dividing surface, while the fourth one is located in inner, bulklike environments. The coordination between the electron and water shows modifications that would suggest a gradual change from the bulk linear hydrogen bond connectivity toward a more marked alignment of the water dipoles along the electron−water radial direction. The magnitudes of the fluctuations in both the electron−solvent density fields and the local polarization in the close vicinity of the electron are larger as we approach the interface from the bulk liquid. The presence of the electron promotes an overall radial polarization at the interface over characteristic distances of the order of 3−4 Å away from the position of the electron.

An analysis of the density of bound electronic states shows typically a ground s-like state at ca. −3.5 eV and three p-like excited states lying at ca. −1 eV from the continuum. Compared to the bulk results, the reduction of ∼0.5 eV in the energy gap between the ground state and the rest of the excited states leads to the red-shift in the observed optical absorption spectrum. We hope that the comments of the main conclusions summarized in the previous paragraphs may be corroborated by direct experimental research in the near future.

Acknowledgment. D.L. is a member of Carrera del Investigador Científico de CONICET (Argentina).

References and Notes

(1) Wilson, M. A.; Pohorille, A.; Pratt, L. R. *Chem. Phys. Lett.* **1989**, *129*, 209.
(2) Benjamin, I. *J. Chem. Phys.* **1991**, *95*, 3698.
(3) Stuart, S. J.; Berne, B. J. *J. Phys. Chem. A* **1999**, *103*, 10300.
(4) Jungwirth, P.; Tobias, D. J. *J. Phys. Chem. B* **2000**, *104*, 7702. Jungwirth, P.; Tobias, D. J. *J. Phys. Chem. A* **2002**, *106*, 379. Jungwirth, P.; Tobias, D. J. *J. Phys. Chem. B* **2002**, *106*, 6361. Tobias, D. J.; Jungwirth, P.; Parrinello, M. *J. Phys. Chem.* **2001**, *114*, 7036. Salvador, P.; Curtis, J. E.; Tobias, D. J.; Jungwirth, P. *Phys. Chem. Chem. Phys.* **2001**, *105*, 654.
(5) Benjamin, I. *Chem. Rev.* **1996**, *96*, 1449.
(6) *Biomembrane Electrochemistry*; Blank, M., Vodyanoy, I., Eds.; Advances in Chemistry Series, Vol. 235; American Chemical Society: Washington, DC, 1994.
(7) *The Chemistry of Acid Rain*: *Sources and Atmospheric Processes*; Johnson, R. W., Gordnon, G. E., Eds.; ACS Symposium Series, Vol. 349; American Chemical Society: Washington, DC, 1987.
(8) Gratzel, M. *Heterogeneous Photochemical Electron Transfer*; CRC Press: Boca Raton, FL, 1989.
(9) Adamson, A. W. *Physical Chemistry of Surfaces*; Wiley: New York, 1990.
(10) Gragson, D. E.; Richmond, G. L. *J. Am. Chem. Soc.* **1998**, *120*, 366.
(11) Richmond, G. L. *Chem. Rev.* **2002**, *102*, 2693.
(12) Gragson, D. E.; McCarty, B. M.; Richmond, G. L. *J. Am. Chem. Soc.* **1996**, *110*, 14272. Gragson, D. E.; McCarty, B. M.; Richmond, G. L. *J. Am. Chem. Soc.* **1997**, *119*, 6144.
(13) Zimdar, D.; Eisenthal, K. B. *J. Phys. Chem. A* **1999**, *103*, 10567. Zimdar, D.; Eisenthal, K. B. *J. Phys. Chem. B* **2001**, *105*, 3993. Benderskii, A. V.; Eisenthal, K. B. *J. Phys. Chem. B* **2001**, *105*, 6698. Benderskii, A. V.; Eisenthal, K. B. *J. Phys. Chem. A* **2002**, *106*, 7482.
(14) Baldelli, S.: Mailhot, G.; Ross, P. N.; Shen, Y. R.; Somorjai, G. A. *J. Phys. Chem. B* **2001**, *105*, 654.
(15) Morita, A.; Hynes, J. T. *Chem. Phys.* **2000**, *258*, 371. Morita, A.; Hynes, J. T. *J. Phys. Chem. B* **2002**, *106*, 673.
(16) Benjamin, I. *Phys. Rev. Lett.* **1994**, *73*, 2083.
(17) Wilson, K. R.; Schaller, R. D.; Co, D. T.; Saykally, R. J.; Rude, B. S.; Catalano, T.; Bozek, K. D. *J. Chem. Phys.* **2002**, *117*, 7738. Wilson, K. R.; Cavalleri, M.; Rude, B. S.; Schaller, R. D.; Nilsson, A.; Petterson, L. G. M.; Goldman, N.; Catalano, T.; Bozek, K. D.; Saykally, R. J. *J. Phys.*: *Condens. Matter* **2002**, *14*, L221.
(18) Giraud, V.; Krebs, P. *Chem. Phys. Lett.* **1982**, *86*, 85. Krebs, P.; Heintze, M. *J. Chem. Phys.* **1982**, *76*, 5484.
(19) Hart, E. J.; Anbar, M. *The Hydrated Electron*; Wiley: New York, 1970.
(20) Jortner, J.; Kestner, N. R. *Electrons in Fluids*; Springer: New York, 1973.
(21) Sprik, M.; Impey, R. W.; Klein, M. L. *J. Stat. Phys.* **1986**, 43, 949.
(22) Wallqvist, A.; Thirumalai, D.; Berne, B. J. *J. Phys. Chem.* **1987**, *86*, 6404.
(23) Schnitker, J.; Rossky, P. J. *J. Chem. Phys.* **1987**, *86*, 3462.
(24) Schnitker, J.; Rossky, P. J. *J. Chem. Phys.* **1987**, *86*, 3471.
(25) Turi, L.; Borgis, D. *J. Chem. Phys.* **2002**, *117*, 6186.
(26) Laria, D.; Wu, D.; Chandler, D. *J. Chem. Phys.* **1991**, *95*, 4444.
(27) Jou, F.-Y.; Freeman, G. R. *J. Phys. Chem.* **1977**, *81*, 909.
(28) Silva, C.; Wakhout, P. K.; Yokohama, K.; Barbara, P. F. *Phys. Rev. Lett.* **1998**, *80*, 1086. Gaudel, Y.; Pommeret, S.; Migus, A.; Yamada, N.; Antonetti, A. *J. Am. Chem. Soc.* **1990**, *112*, 2925. Long, F. H.; Lu, H.; Eisenthal, K. B. *Phys. Rev. Lett.* **1990**, *64*, 1469.
(29) Wallqvist, A.; Martyna, G.; Berne, B. J. *J. Phys. Chem.* **1988**, *92*, 1721.
(30) Nicolas, C.; Boutin, A.; Lévy, B.; Borgis, D. *J. Chem. Phys.* **2003**, *118*, 9689.
(31) Romero, C.; Jonah, C. D. *J. Chem. Phys.* **1989**, *90*, 1877.
(32) Jou, F.-Y.; Freeman, G. R. *J. Phys. Chem.* **1979**, *83*, 2383.
(33) Michael, B. D.; Hart, E. J.; Schmidt, K. *J. Phys. Chem.* **1971**, *75*, 2798. Wu, G.; Katsumura, Y.; Muroya, Y.; Li, X.; Terada, Y. *Chem. Phys. Lett.* **2000**, *325*, 351; *Radiat. Phys. Chem.* **2001**, *60*, 395.
(34) (a) Bartels, D. M.; Cline, J. A.; Jonah, C. D.; Takahashi, K. *Abstracts of Papers*, *Part 2*, 222nd National Meeting of the American Chemical Society, Chicago, IL, Aug 26−30, 2001; American Chemical Society: Washington, DC, 2001; 263-PHYS. (b) Cline, J. A.; Jonah, C. D.; Bartels, D. M. The Solvated Electron in Supercritical Water: Spectra, Yields, and Reactions. SCR-2000, Proceedings of the First International Symposium in Supercritical Water-cooled Reactors, Design, and Technology, The University of Tokyo, Tokyo, Japan, 2000.
(35) Gaathon, A.; Czapski, G.; Jortner, J. *J. Chem. Phys.* **1972**, 58, 2648. Jortner, J.; Gaathon, A. *Can. J. Chem.* **1977**, *55*, 1801.
(36) Dimitrijevic, N. M.; Takahashi, K.; Bartels, D. M.; Jonah, C. D. *J. Phys. Chem. A* **2001**, *105*, 7236.
(37) Laria, D.; Skaf, M. S. *J. Phys. Chem. A* **2002**, *106*, 8066.
(38) Wallqvist, A.; Thirumalai, D.; Berne, B. J. *J. Phys. Chem.* **1986**, *85*, 1585.
(39) Barnett, R. N.; Landman, U.; Cleveland, C. L. *Phys. Rev. Lett.* **1987**, *59*, 811.
(40) Barnett, R. N.; Landman, U.: Cleveland, C. L.; Jortner, J. *J. Chem. Phys.* **1988**, *88*, 4421. Barnett, R. N.; Landman, U.: Cleveland, C. L.; Jortner, J. *J. Chem. Phys.* **1988**, *88*, 4429.
(41) Grimes, C. C.; Brown, T. R. *Phys. Rev. Lett.* **1974**, *32*, 280.
(42) Cole, M. W. *Rev. Mod. Phys.* **1974**, *46*, 451. Chen, E.; Cole, M. W.; Cohen, M. H. *Phys. Rev. B* **1994**, *50*, 1136.
(43) Hernandez, J. P. *Rev. Mod. Phys.* **1991**, *63*, 675.
(44) Saville, G. F.; Goodkind, J. M.; Platzman, P. M. *Phys. Rev. Lett.* **1993**, *70*, 1517.
(45) Ge, N.-H.; Wong, C. M.; Harris, C. B. *Acc. Chem. Res.* **2000**, *33*, 111.
(46) Miller, A. D.; Bezel, I.; Gaffney, K. J.; Garret-Roe, S.; Liu, S. H.; Szymanski, P.; Harris, C. B. *Science* **2002**, *297*, 1163.
(47) Liu, S. H.; Miller, A. D.; Gaffney, K. J.; Szymanski, P.; Garret-Roe, S.; Bezel, I.; Harris, C. B. *J. Phys. Chem. B* **2002**, *106*, 12908.
(48) Harris, C. B.; Ge, N.-H.; Lingle, R. L., Jr.; McNeil, J. D.; Wong, C. M. *Annu. Rev. Phys. Chem.* **1997**, *48*, 711.
(49) Ge, N.-H.; Wong, C. M.; Linge, R. L., Jr.; McNeill, J. D.; Gaffney, K. J.; Harris, C. B. *Science* **1998**, *279*, 202.
(50) Snee, P. T.; Garrett-Roe, S.; Harris, C. B. *J. Phys. Chem. B* **2003**, *107*, 13608.
(51) Turi, L.; Gaigeot, M.-P.; Levy, N.; Borgis, D. *J. Chem. Phys.* **2001**, *114*, 7805.
(52) Berendsen, H. J. C.; Postma, J. P. M.; Von Gunsteren, W. F.; Hermans, J. *Intermolecular Forces*; Reidel: Dordrecht, 1981.
(53) Yeh, I.-C.; Berkowitz, M. L. *J. Chem. Phys.* **1999**, *111*, 3155.
(54) Feynman, R. P. *Statistical mechanics*; Addison-Wesley: Reading, 1972.
(55) Chandler, D.; Wolynes, P. G. *J. Chem. Phys.* **1981**, *74*, 4078.
(56) Rodriguez, J.; Skaf, M. S.; Laria, D. *J. Phys. Chem.* **2003**, *119*, 6044.
(57) Pohorille, A.; Benjamin, I. *J. Chem. Phys.* **1991**, *94*, 5599.
(58) Nichols, A. L., III; Chandler, D.; Singh, Y.; Richardson, D. *J. Chem. Phys.* **1984**, *81*, 5109.
(59) Rigorously, the average value of $\cos(\theta_i^z)$ at the clean water/air interface is not zero (see: Towsend, R. M.; Rice, S. A. *J. Chem. Phys.* **1991**, *94*, 2207). However, for the purposes of the present discussion, the limiting value of $G_j^z(r = \infty)$ can be safely neglected.